Small-scale variability of the cross-shelf flow over the outer shelf of the Ross Sea

Josh Kohut,[1] Elias Hunter,[1] and Bruce Huber[2]

Received 31 May 2012; revised 11 December 2012; accepted 17 January 2013; published 10 April 2013.

[1] The importance of cross-shelf transport across the Ross Sea on local and remote processes has been well documented. In the Ross Sea, mid-water intrusions of Circumpolar Deep Water (CDW) are modified by shelf water near the shelf break to form Modified Circumpolar Deep Water (MCDW). In 2010–2011, we deployed multi-platform technologies focused on this MCDW intrusion in the vicinity of Mawson and Pennell Banks to better understand its role in ecosystem processes across the shelf. The high-resolution time and space sampling provided by an underwater glider, a short-term mooring, and a ship-based survey highlight the scales over which these critical cross-shelf transport processes occur. MCDW cores were observed as small-scale well-defined features over the western slopes of Pennell and Mawson Banks. The mean transport along Pennell Bank was estimated to be about 0.24 *Sv* but was highly variable in time (hours to days). The observations suggest that the core of MCDW is transported by a predominately barotropic flow that follows topography around the banks toward the south until the slope of the bank flattens and the warmer water moves up and over the bank. This pathway is shown to link the source MCDW with an area of high productivity over the shallows of Pennell Bank.

Citation: Kohut, J., E. Hunter, and B. Huber (2013), Small-scale variability of the cross-shelf flow over the outer shelf of the Ross Sea, *J. Geophys. Res. Oceans, 118*, 1863–1876, doi:10.1002/jgrc.20090.

1. Introduction

[2] The shelves of Antarctica's continental seas are critical centers for water mass transformation. The water masses that undergo these transformations have origins in the deep ocean and on the shelf itself [*Foster and Carmack*, 1976; *Killworth*, 1977; *Baines and Condie*, 1998]. The seasonal cycle of the high latitudes plays an important role in their formation, transformation, and exchange between the shallow shelves and the deep waters of the Southern Ocean [*Assmann et al*., 2003; *Assmann and Timmermann*, 2005]. In the winter, strong katabatic winds streaming off the Antarctic continent maintain open water polynas with nearly continuous ice formation [*Budillon and Spezie*, 2000; *Fusco et al*., 2009]. The newly formed dense water mixes completely to the bottom and eventually becomes Antarctic Bottom Water (AABW) [*Orsi et al*., 1999; *Gordon et al*., 2009b]. AABW is a key component of the global climate system, bringing cold, recently ventilated water to lower latitudes [*Orsi, et al*., 2002; *Jacobs*, 2004]. The austral summer brings warmer temperatures, weaker winds, and nearly continuous solar radiation. This leads to a more stratified water column with a cold fresher layer over the dense bottom water formed the winter seasons before. In the Ross Sea, relatively warm Circumpolar Deep Water (CDW) originating off the shelf preferentially intrudes onto the shelf at sites where the bottom topography changes direction relative to the coastal flow [*Klinck and Dinniman*, 2010]. The CDW then mixes with these shelf water masses at the shelf break to form Modified Circumpolar Deep Water (MCDW) [*Whitworth et al*., 1998]. With neutral densities between 28 and 28.27 [*Orsi and Wiederwohl*, 2009], these intrusions move onto the shelf as mid-water features sandwiched between the dense bottom and lighter surface water masses. This large mass of water injects onto the shelf as mid-water features at specific locations, bringing with it nutrients and heat [*Dinniman et al*., 2003; *Hiscock*, 2004; *Smith et al*., 2006]. The interaction, mixing, and exchange of these water masses helps to maintain deep ocean heat exchange, ventilation, and important ecosystems processes like seasonal blooms [*Arrigo et al*., 2008; *Budillon et al*., 2011; *Fragoso and Smith*, 2012]. While these coastal seas are typically small in area, the role that they play in the exchange of water masses between the shelf and open ocean has important implications to both the global circulation and the critical ecosystem it supports.

[3] Compared to other coastal seas surrounding Antarctica, the Ross Sea in the Pacific sector of the Southern Ocean is relatively well sampled (Figure 1). Following *Orsi and Wiederwohl* [2009], we characterize the water masses of the Ross Sea based on their neutral densities as follows: (1) dense bottom water (neutral densities greater than 28.27), (2) MCDW/CDW (neutral densities between 28.0 and 28.27),

[1]Institute of Marine and Coastal Sciences, Rutgers University, New Brunswick, New Jersey, USA.
[2]Lamont Doherty Earth Observatory, Columbia University, Palisades, New York, USA.

Corresponding author: J. Kohut, Institute of Marine and Coastal Sciences, Rutgers University, 71 Dudley Road, New Brunswick, NJ 08901, USA. (kohut@marine.rutgers.edu)

2169-9275/13/10.1002/jgrc.20090

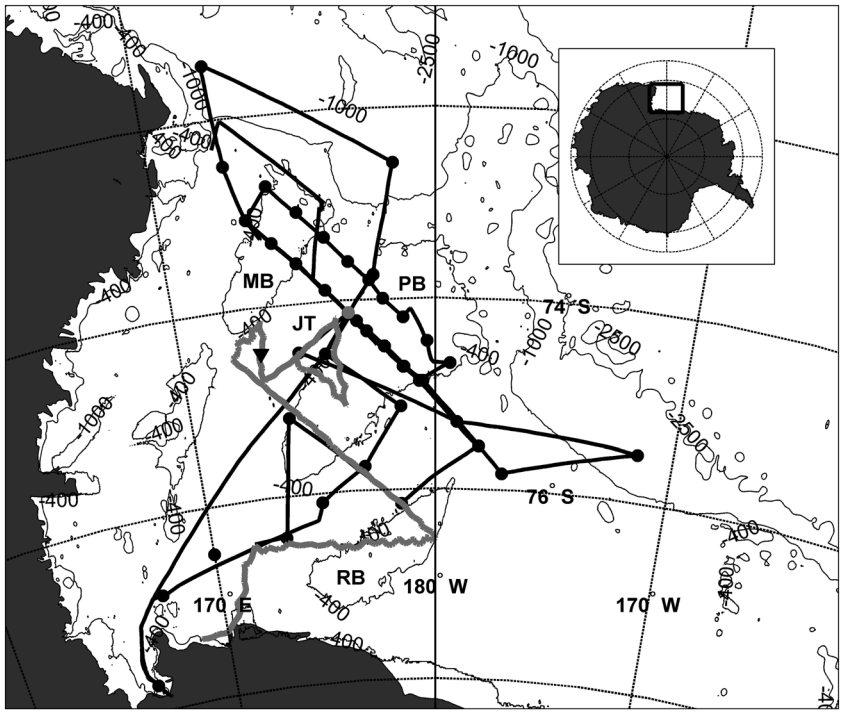

Figure 1. Map of the study site in the Western Ross Sea showing the ship track (black line), ship stations (black dots), glider track (gray line), and mooring location (gray dot). Isobaths highlight the relevant topographic features including Ross Bank (RB), Pennell Bank (PB), Joides Trough (JT), and Mawson Bank (MB). The black triangle indicates the glider's location at the start of the ship survey.

and (3) surface water with neutral densities less than 28.0 (Figure 2). The distribution of these water masses has been described in the context of available data primarily from ship surveys and moorings. In the western Ross Sea, dense High Salinity Shelf Water (HSSW) sinks to the seafloor and splits with a southward branch going under the Ross Ice Shelf and a northward branch heading toward the shelf break. The asymmetry of the deep water formation centers across the entire sea sets up an east/west density gradient with denser water under the formation centers to the west [*Jacobs and Giulivi*, 1998; *Rickard et al*., 2010]. The weaker winds and warmer temperatures of the Austral summer stratify the western Ross Sea with a layer of fresher water capping the HSSW formed the seasons before. As the small winter polyna grows to open the entire Ross Sea, blooms of phytoplankton form the base of the food web. It has been suggested that these blooms are maintained in part by the delivery of macro- and micro-nutrients from the deep water off the shelf [*Hiscock*, 2004; *Fragoso and Smith*, 2012]. In

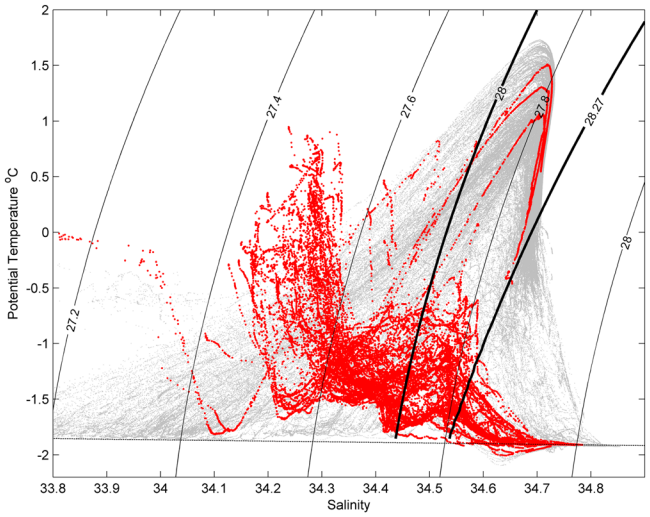

Figure 2. Potential temperature and salinity data for stations sampled by the *RVIB Nathaniel B. Palmer* from 2000 to 2005 (gray) and the SEAFAReRS cruise in 2011 (red). Isopycnals (thin black) and the neutral density bounds of 28.0 and 28.27 for MCDW (thick black) defined by *Orsi and Weiderwhol* [2009] are also shown.

addition to the nutrient supply, this warmer deep water is a source of heat that impacts the rate of sea ice formation and melt through the seasons and could impact the rate of basal melt below the ice shelf if it reaches far enough south.

[4] The Ross Sea shelf break is a critical region for both the exchange of bottom water that moves down the slope and eventually forms dense AABW [*Gordon et al*., 2009a] and the injection of warm CDW that comes from the mid-depths of the Southern Ocean. Both the deep water formed on the shelf and the mid-water of the deep ocean are modified as they move across the shelf break by local mixing processes [*Whitworth et al*., 1998; *Robertson et al*., 2003]. The most energetic process that likely contributes to this mixing is the tides. The tides of the Ross Sea are predominately diurnal with higher amplitudes over the shallow banks and along the shelf break [*Robertson*, 2005; *Whithworth and Orsi*, 2006; *Padman et al*., 2009]. The tides interact with the varying topography and the background flow along the shelf break toward the west to mix and modify the water masses before they move away from the shelf break [*Dinniman et al*., 2003; *Gordon et al*., 2009a]. The dominant advective feature along the shelf break is the mostly westward jet maintained by the density gradient across the shelf break. Instabilities and interactions of this jet with the underlying topography lead to preferential centers of CDW intrusions onto the shelf [*Klinck and Dinniman*, 2010].

[5] While this shelf break region is undersampled, both observations and numerical studies have identified its importance to the north/south exchange of water masses. These studies are based on observations collected during intensive surveys and mooring deployments [e.g., *Gordon et al*., 2009a] and numerical models verified by either the direct observations [e.g., *Dinniman et al*., 2003] or climatologies determined from the observations [e.g., *Klinck and Dinniman*, 2010]. In the early 2000s, a field program was conducted as part of the AnSlope project [*Gordon et al*., 2009a] with ship surveys and mooring deployments focused on the shelf break near Drygalski Trough in the northwest Ross Sea. These critical observations have shown the importance of the shelf break as the basis for the formation of the dense water that sink and form AABW [*Muench et al*., 2009; *Gordon et al*., 2009b]. These papers cite the importance of the tides in not only mixing the parent water masses of the Ross Sea but also modulating the position of the shelf break jet. The north south movement of this jet by the tides may facilitate the exchange of dense water off the shelf and into the deep sea along the seafloor. Similarly, the variability of this jet and its interaction with the underlying topography likely control the variability observed in the movement of CDW onto the shelf [*Dinniman et al*., 2003]. At specific locations along the shelf break, sharp changes in the orientation of the isobaths along the general path of the shelf break jet lead to preferential locations for intrusions of the jet onto the shelf. The models show that these regions of consistent upwelling of CDW coincide with sharp turns toward the north in front of the flow. One region of preferential upwelling is offshore of Joides Trough between Mawson and Pennell Banks (Figure 1). Virtual dye experiments within the modeled current fields identify Joides and Drygalski Troughs as regions of consistent MCDW intrusions. *Dinniman et al*. [2003] suggest that once this CDW is up on the shelf, it mixes with the surrounding shelf water and moves south along the eastern side of Joides trough toward the interior of the shelf.

[6] In this study, we use an extensive multi-platform observation array to characterize the southward flow of MCDW from the shelf break to the interior of the Ross Sea Shelf as part of the Slocum Enhanced Adaptive Fe Algal Research in the Ross Sea (SEAFAReRS) project. The sampling is focused on the western slope of Pennell Bank along the eastern edge of Joides Trough shoreward of the shelf break and the CDW mixing sites associated with the shelf break jet. Particular emphasis on the small time and space scales of the MCDW intrusion drove the sampling design. A ship survey, glider Autonomous Underwater Vehicle (AUV) mission, and a mooring deployed at a depth of 400 m are used to characterize the spatial and temporal variability of the southward flow of MCDW. Section 2 describes the platforms and available data, and section 3 presents the results. Implications and concluding remarks are discussed in sections 4 and 5, respectively.

2. Data

2.1. Glider AUV

[7] A deep Slocum electric glider manufactured by Teledyne Webb Research was deployed. The buoyancy-driven propulsion of the glider AUV affords high-efficiency and deployment endurance [*Schofield et al*., 2007]. Throughout the mission, the glider moved in a sawtooth pattern between 10 m below the surface and 10 m above the bottom determined from onboard pressure and altimeter data. This glider was equipped with a sensor suite that characterized the ecosystem's physical structure (conductivity, temperature, depth, and dissolved O_2), in situ phytoplankton fluorescence and optical backscatter. On 10 December 2010, the deep glider was deployed from the sea ice edge near Ross Island. The 52 day mission took the glider east along 76.5°S before turning toward the northwest over Ross Bank (Figure 1). The glider then completed a cross section of Pennell Bank, Joides Trough, and up the eastern slope of Mawson Bank before heading back east toward Pennell Bank. The glider began this section near Ross Bank on 28 December 2011 and completed the section 13 days later near Mawson Bank on 10 January 2011. Nine days before the ship left the dock, these data helped guide the initial ship sampling plan with a high-resolution section of temperature, salinity, density, and dissolved oxygen (Figure 3). Once the ship started its survey on 10 January 2011, the complimentary glider sampling provided high vertical and horizontal resolutions of the physical characteristics in the vicinity of the flow along western Pennell Bank and into Joides Trough. The glider was recovered on 4 February toward the end of the ship survey. The CTD resolution was 0.25 m in the vertical and approximately 2.2 times the water depth in the horizontal. The CTD data were verified against the ship's data during two calibration casts with the glider secured to the ship's rosette.

2.2. Ship Surveys

[8] A ship survey was completed aboard the *RVIB Nathaniel B. Palmer* (NBP). The ship left McMurdo Station on 20 January 2011 on a 26 day cruise across the Ross Sea.

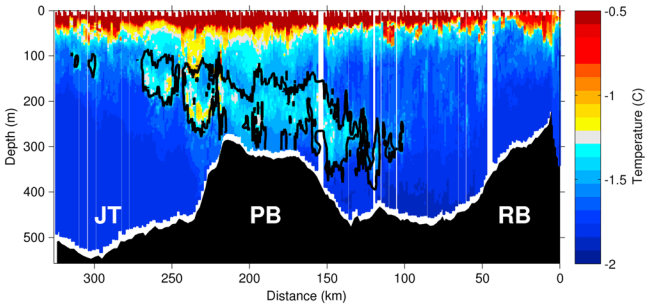

Figure 3. Glider cross section of potential temperature sampled between Ross Bank and Joides Trough. The black contour is the 5.1 ml/L dissolved oxygen isopleth showing the oxygen minimum coincident with the sub-surface temperature maximum associated with MCDW. The topographic features are labeled as in Figure 1.

The sampling focused on the banks and troughs of the outer shelf in the western Ross Sea (Figure 1). Throughout the cruise, underway measurements of temperature and salinity were taken every second with the NBP thermosalinograph at an intake depth of 6.7 m below the surface. These data were sub-sampled every 10 s along the ship's track. Vertical profiles of velocity were sampled by a ship mounted downward looking 150 KHz Acoustic Doppler Current Profiler (ADCP). These shipboard data were processed with the University of Hawaii Data Acquisition System (UHDAS) software. Five minute ensembles were collected with a vertical bin resolution of 8 m. Raw depth-averaged and depth-dependent data were de-tided using the predicted barotropic tide derived from Ross Sea sub-region of the Oregon Tidal Prediction System (Figure 4) [*Erofeeva et al.*, 2005].

[9] In addition to the underway data, the ship survey completed 79 stations (Figure 1). At each station, at least one full water column profile of the ship's CTD rosette was completed. All stations were sampled at least once with more frequent repeat stations along the southern line crossing both Pennell and Mawson Banks. The Sea-Bird CTD mounted on the rosette was calibrated before and after the cruise. Our analysis will focus in on a single along-bank section from off the shelf to the southern end of Pennell Bank and eight repeat cross sections across Pennell Bank, Joides Trough, and Mawson Bank (Figure 1). The distribution of the potential temperature and salinity sampled over these stations is shown in Figure 2.

2.3. Mooring Deployment

[10] A surface-buoyed mooring was deployed on 27 January 2011 for 13 days on the western side of Pennell Bank (Figure 1). It was anchored to the bottom on 600 m of mooring wire in water 400 m deep. After recovery from a 3 year deployment as part of the Cape Adare Long-term Moorings (CALM) project earlier in the cruise, the sensors were quickly repurposed for this short redeployment focused on the MCDW intrusion. The

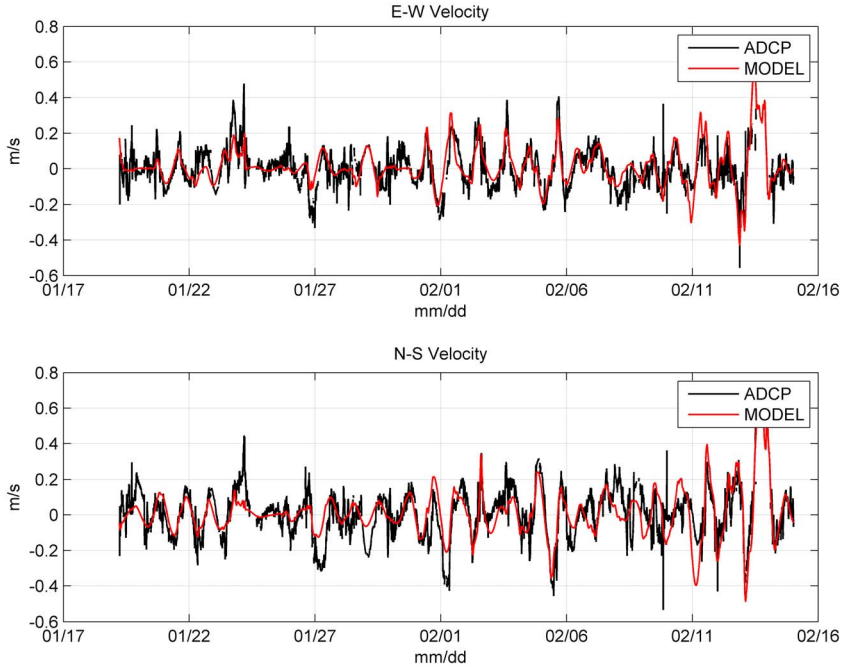

Figure 4. Time series of depth-averaged velocity in the east (top) and north (bottom) components from the NBP hull mounted ADCP (black) and matched tidal velocity estimated from the barotropic tide model Ross_TIM [*Erofeeva et al.*, 2005] (red).

sensor distribution and mooring location were determined from by available ship and glider data to target the MCDW core flowing south along the western slope of Pennell Bank. Four depths were instrumented: 50 m (current meter with temperature and pressure), 225 m (current meter with temperature and pressure), 230 m (salinity, temperature and pressure), and 300 m (temperature and pressure). The two mid-water depths (225 m and 230 m) specifically targeted the MCDW water observed by the glider and ship survey. All instruments sampled every 5 min. Current meter magnetic compasses were corrected for the local magnetic declination of 112°.

3. Results

[11] A single glider section across the bank and trough topography of the Ross Sea shows the scale and possible dynamics driving the distribution of MCDW (Figure 3). The glider began the section on 28 December 2010 over Ross Bank and reached Joides Trough on 10 January 2011. The glider section identifies the relatively warmer potential temperature (greater than approximately −1.3°C) and minima in dissolved oxygen indicative of MCDW over the western slope of Pennell Bank and suggests that the core of MCDW mixes up and over the shallows of the bank (Figure 3). The location of the warmer water feature identified through the real-time data feeds from the glider guided the sampling strategy initiated on 19 January 2011 when the NBP left the pier at McMurdo Station. Unlike previous surveys conducted in the Ross Sea, the sampling design centered on this small feature seen on the glider section with repeat ship sections across the bank and subsequent mooring deployment in the core to resolve the relevant time and space scales.

[12] For this study, the observations are organized into along- and cross-bank sections. The along-bank direction was determined to be 20° clockwise from true north based on the largest bathymetric gradient over a scale of 0.5° in latitude (5.5 km) and longitude (1.7 km). In all of the figures, positive indicates flow toward the northeast (20°) and southeast (110°) for the along- and across-bank components, respectively.

3.1. Along-Bank Structure of the MCDW Intrusion

[13] The hydrographic data along the bank was taken over a series of five stations (Figure 5). The southernmost station (#2) was sampled early in the cruise based on initial guidance from the glider locating a core of MCDW along the western slope of Pennell Bank. Six days later, the along-bank section continued with a series of stations beginning off the shelf and moving south along Pennell Bank (stations 14–17, all sampled within 1.5 days of each other). For each station, we show the average profile of the upper 400 m (Figure 6). The gray-shaded region is the portion of the water column in which the neutral density fall within the range set for MCDW as defined in *Orsi and Wiederwohl* [2009]. The potential temperature-salinity plots below each profile are the data for that particular station in red plotted against all the data collected on the cruise in gray. At all the stations, there is a well-defined surface layer of warmer fresher water primarily associated with the melting of the seasonal sea ice and subsequent solar heating (Figure 6). Distinction between the stations is seen in the depth and strength of the thermal gradient between the surface layer and the cooler layer just below. Off the shelf break at the deep water station (14), the warmer CDW is seen at depths deeper than 300 m. Based on the Θ-S characteristics, this station has two clear water masses, a warmer fresh layer within the upper 70 m and the warmer saltier CDW layer below. On the inshore side of the shelf break at station 15, the deep water peak in potential temperature seen in station 14 cools and freshens as it mixes with shelf water, forming MCDW. Continuing south along the bank, the subsequent stations show that dilution of the pure CDW signal seen offshore (station 14) and a general increase in the potential temperature of the surface layer, likely driven by the earlier melt of the seasonal sea ice leading to longer exposure to solar heating. While the depth and vertical extent of the MCDW varies from station to station, this water lay within a broad range of depths between 200 m to 350 m deep.

[14] The velocity data identify how these water masses move across the shelf. Both the depth-averaged and depth-dependent velocity data show a significant rotation in the currents as the ship moved from the deep water off the shelf break southwest along the western slope of Pennell Bank (Figure 7). To the north, the depth-averaged flow of the shelf break jet peaks over the steep slope of the shelf break with a broad shoulder extending south over the shelf. Further to the south, the currents rotate counterclockwise to an approximate along-bank direction in the vicinity of the 400 m isobath west of Pennell Bank. The shelf break jet has a sub-surface velocity peak of about −0.3 m/s 100 m deep at about 73.25°S (Figure 7,

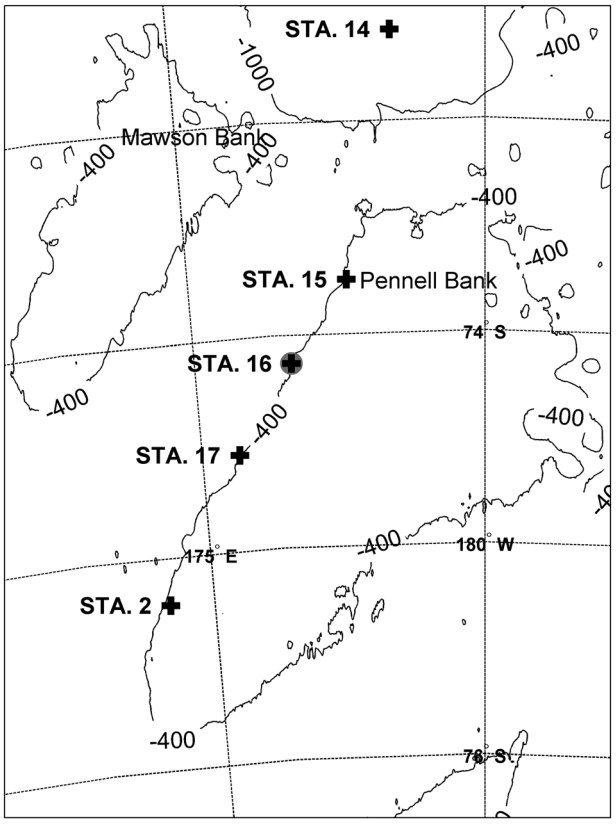

Figure 5. Map showing the ship stations (black cross) included in the along-bank section. The mooring location is shown as a small gray circle.

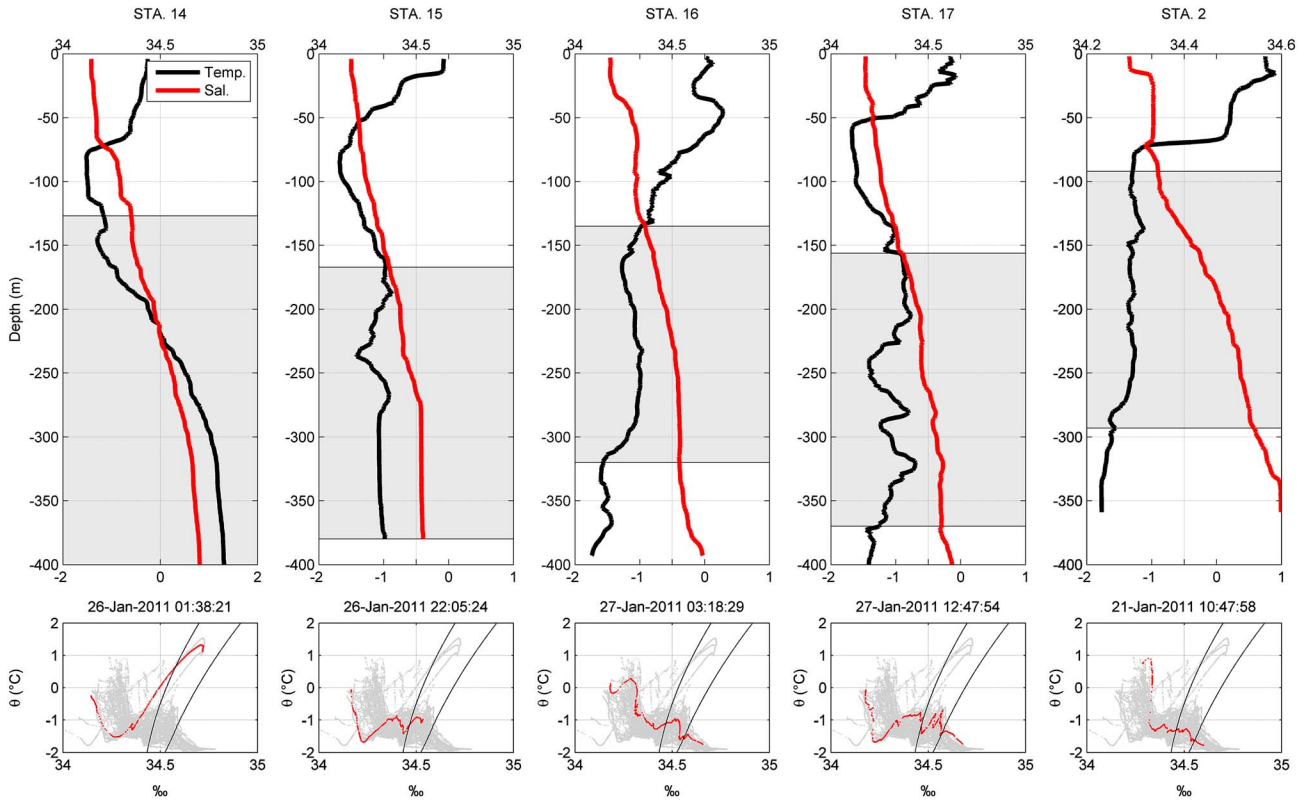

Figure 6. The average potential temperature (black) and salinity (red) for each station in the along-bank line. Vertical distributions of the neutral densities that define MCDW are shaded gray for each station. Below each section, the potential temperature-salinity plot is shown for all stations (gray) and that particular station (red). The neutral density bounds for MCDW are shown as thick black lines.

upper right). The along-bank flow further south is stronger with the strongest velocities exceeding 0.3 m/s in the upper 200 m of the water column.

3.2. Across-Bank Structure of the MCDW Intrusion

[15] Over the course of the cruise, the ship made eight repeat transects across Pennell Bank and Joides Trough (Figure 1). Along this cross section of the banks, we sampled nine stations, five over Pennell Bank, three over Mawson Bank, and one over Joides Trough (Figure 8). At each station, there were at least three CTD casts with a maximum of eight casts sampled at our mooring station over the 400 m isobath along the western slope of Pennell Bank. For each of these stations, we show the Θ-S diagrams for the casts taken at that station (red) relative to all stations sampled throughout the cruise (gray). The warmer fresher surface layer resulting from the sea ice melt earlier in the season and subsequent solar heating is seen across all stations with the warmest surface water over the shallows of the banks. The strongest MCDW signal is seen near Joides Trough and the western slope of Pennell and Mawson Banks, coincident with our mooring site over the 400 m isobath. The deep HSSW is only seen in stations at least 400 m deep.

[16] The mean cross section based on all the casts taken at each station shows the significant variation in water column properties across the complicated topography. There is a clear surface layer of warmer fresher water across the entire section with slightly fresher water over the western slopes of the banks (Figure 9). Below this roughly 80 m deep surface layer, there is significant variability in the distribution of the deeper water masses. At depth in Joides trough, there is a thick layer of dense shelf water reaching up from the bottom to a depth of about 250 m. At mid-depth, the most striking feature is the slug of warmer MCDW centered over the 400 m isobath above the western slope of Pennell Bank. The small region of MCDW is confined to a depth between 180 m and 250 m and is not seen in the neighboring stations. While there is evidence of a similar slug of MCDW over the western slope of Mawson Bank, its potential temperature and oxygen signal are more dilute and spread over a wider range of depths. The contrasting MCDW characteristics between the two banks are likely due to the more energetic tides over the narrower Mawson Bank. This section is consistent with the structure of the MCDW seen by the glider several weeks before with a core of MCDW over the 400 m isobath except that in this section, this warmer water does not extend east over the shallows of the bank (Figures 3 and 9). Unlike the glider section further south, this section completed closer to the shelf break clearly shows the presence of warmer deep water over the slope isolated from the shallows of the bank.

[17] The repeat sections of underway ADCP data describe the movement of these water masses across the shelf. The depth-averaged flow averaged over all eight cross sections shows a clear link to topography with the southward flow over the western slopes of Mawson and Penell Banks and the northward flow along the eastern slope of Mawson Bank (Figure 10, left). For both banks, the flow is about −0.3 m/s and centered just inside the

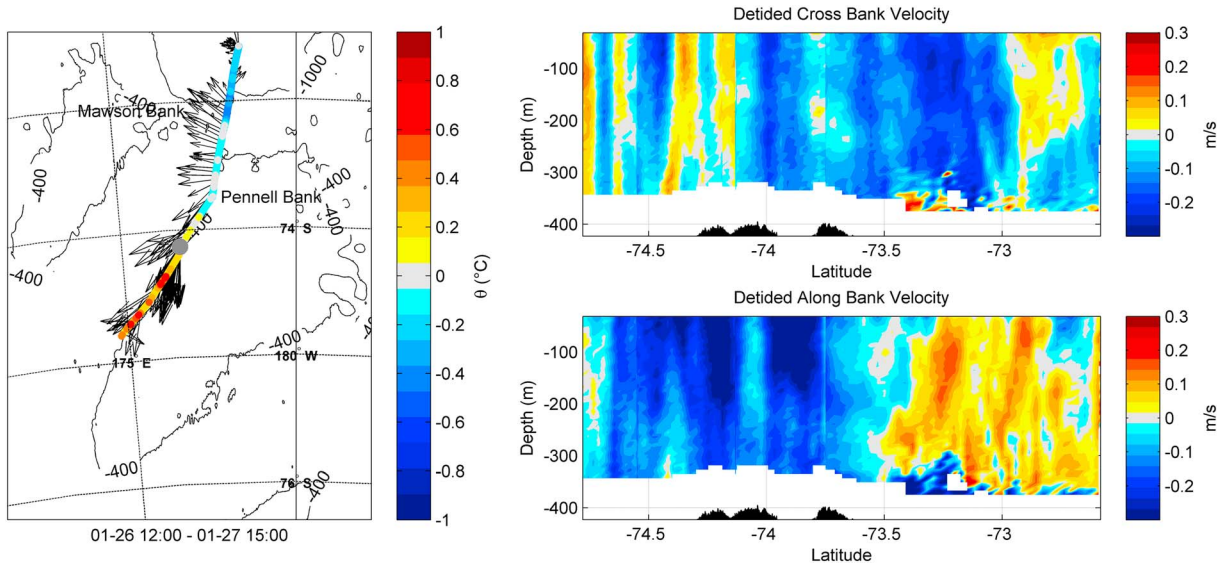

Figure 7. De-tided depth-averaged currents (m/s, black vectors) and surface temperature (colored track) over the along-bank section (left). The depth-dependent velocity sections for the cross-bank (above right) and along-bank (below right) velocity components. The mooring location is shown as a gray circle (left).

400 m isobaths. There is also a second region of southward flow centered over Joides Trough.

[18] The depth-dependent velocity data averaged across all eight cross sections of the banks show the largest vertical shear in the along-bank flows to the north and south over the eastern and western slopes of the banks, respectively. The southward flow along the banks is seen to vary with depth. This mean surface intensified flow of 0.3 m/s decays to about 0.1 m/s at 300 m but never reverses (Figure 10, right). Similarly along the western bank of Mawson, the stronger along-bank velocities are shallower and not as strong as those seen along Pennell. For both banks, this southward flow has a weak upslope component (<0.05 m/s). The upslope velocity is relatively uniform with depth except over Mawson Bank where there is a slight intensification at depth around 225 m deep.

[19] The depth-averaged flow of each individual pass across the banks shows regions of relatively constant and variable flow in time. For all eight sections, the flow over the shallows of the banks shows the most variation (Figure 11). This is particularly evident in the upper four sections sampled almost continuously between 8 February and 12 February. Over Pennell Bank, it transitions from relatively strong northward to periods of weak flow to the south. The most consistent feature across all the individual sections is the southward flow along the western slope of the banks. The depth-averaged flow over both slopes is consistently to the south. From section to section, the character of the flow changes from a relatively narrow jet to a broad feature spreading up toward the shallower depths of the banks.

3.3. Volume Transport Onto the Shelf

[20] Models and sparse observations have identified the importance of topography in steering the transport of MCDW south into the interior of the shelf [*Dinniman et al.*, 2003; *Klinck and Dinniman*, 2010]. Given the location, size, and velocity associated with the MCDW core identified over the western slope of Pennell Bank above, we characterize its transport and variability. Both the glider and ship CTD data identify a small core of MCDW centered over the 400 m isobath characterized by a sub-surface potential temperature maximum, dissolved oxygen minimum, and consistent with the neutral density definitions of *Orsi and Wiederwohl* [2009] (Figures 3 and 9). The depth of the sub-surface peak is about 250 m below the surface but is seen as shallow as 180 m and as deep as 280 m. The MCDW is characteristically warmer than the surrounding shelf water, with lower dissolved oxygen concentrations. These two traits are used in addition to the neutral density bounds defined by *Orsi and Weiderwhol* [2009] to tag water as MCDW.

[21] Using the ADCP and station data from the survey, we estimate a mean volume transport of the layer bounding MCDW (defined by neutral density surfaces as above) along the western slope of Pennell Bank. The height of the layer is estimated from the mean CTD profile taken at the 400 m isobath station. Based on this average profile, the MCDW is seen over 100 m of the water column between 180 m and 280 m deep (Figure 9). The width of the MCDW core was estimated from the ADCP sections. The mean velocity transect averaged across all eight cross sections of the bank shows a clearly defined flow moving south along the western slope of the bank. The width of this jet is approximately 20 km. Therefore, the approximate area of the MCDW layer along the western slope of Pennell bank is approximated as 20 km wide by 100 m high. Using the same ADCP data, we calculate the mean velocity in this sub-section of the average transect to be −0.12 m/s. Based on these data, the estimated transport of MCDW south along Pennell Bank is estimated at 2.4×10^6 m^3/s, or 0.24 *Sv*. Since the concentration of MCDW is not precisely known within the volume used in this estimate, this serves as an upper bound for MCDW transport onto the shelf given our available data.

3.4. Temporal and Spatial Variability of the MCDW Intrusion

[22] This estimate provides a scale for the input of MCDW onto the shelf along Pennell Bank. It does not however

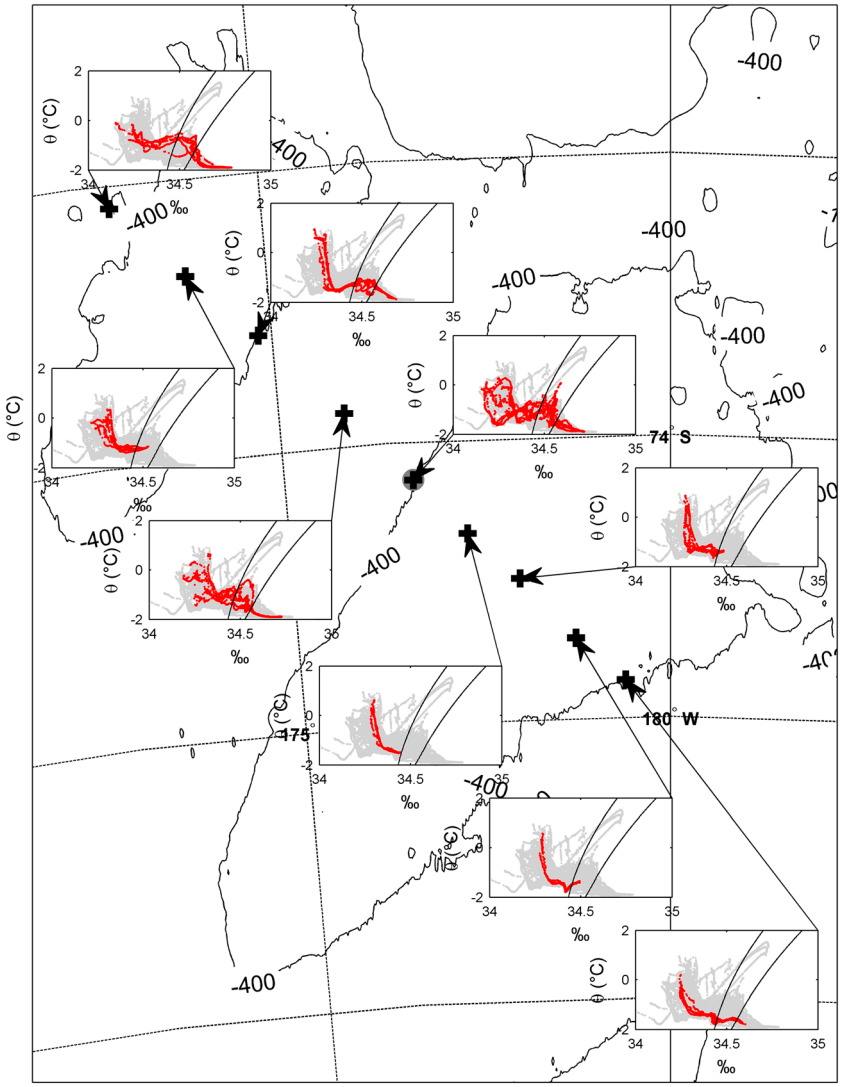

Figure 8. Potential temperature-salinity plots for the cross-bank stations for all stations (gray) and that particular station (red). The neutral density bounds for MCDW are shown as thick black lines. The mooring location (gray circle) is also shown.

adequately represent the significant time and space variability seen in the MCDW core along the banks. The velocity data used to estimate the transport was averaged over eight cross sections of the banks and eight CTD profiles over the 400 m isobath. Both the mooring and glider highlight the variability not captured in this mean estimate of transport. The mooring deployed directly over the 400 m isobath was instrumented at several depths including 225 m and 230 m within the approximate core of MCDW. The 13 day time series shows significant variation in velocity, potential temperature, and salinity. At least 85% of the variability in each velocity component is explained by the strong diurnal tide modulating the along-bank jet in both the along- and across-bank directions. The high-frequency velocity data at 225 m is dominated by the diurnal tide that transitioned from spring to neap over the duration of the deployment. Along-bank flow was consistently toward the southwest at 0.14 m/s, modulated by the tides. The cross-bank flow was upslope at 0.01 m/s, again modulated by the tides. Based on a 25 h running mean, the sub-tidal flow at 225 m depth is relatively steady along isobath throughout the deployment, slightly weakening toward the end of the deployment (Figure 12). The record mean of −0.14 m/s along isobath with a weak upslope component of 0.01 m/s is consistent with the MCDW area mean ADCP value of −0.12 m/s used in the transport calculations in section 3.3.

[23] In addition to the velocity, the potential temperature and salinity sampled at the 230 m depth within the MCDW core had significant variability (Figure 12). Like the velocity, the salinity had a large diurnal signal that ranged from 34.42 to 34.57 through the entire time series. The saltiest water is associated with a weak cross-shore velocity and strong southwestward along-bank velocity. The potential temperature data show a much different response with most of the variation occurring on scales of hours, much shorter than the diurnal signal seen in the velocity and salinity. This is strongest toward the end of 31 January when the potential temperature drops from −0.4° to −1.5° in a few hours. While the potential temperature data were much more variable over a large range of time scales, a diurnal signal was

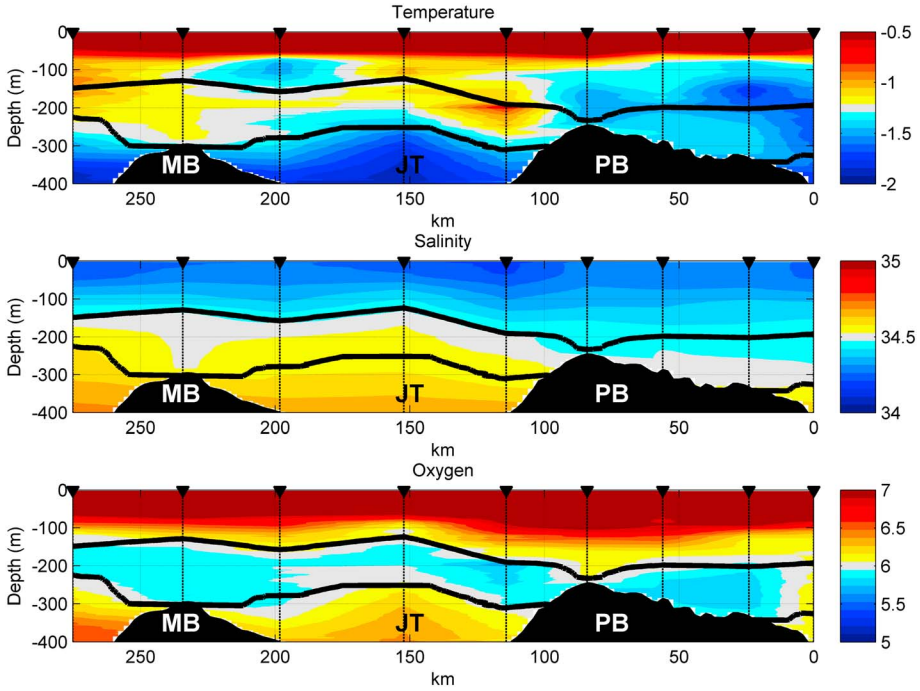

Figure 9. Average cross section of potential temperature (°C, top), salinity (psu, middle), and dissolved oxygen (ml/L, bottom). The stations sampled over the across-bank section are shown as vertical dashed lines. The neutral density bounds defining MCDW are shown in black, and the topographic features are labeled as in Figure 1.

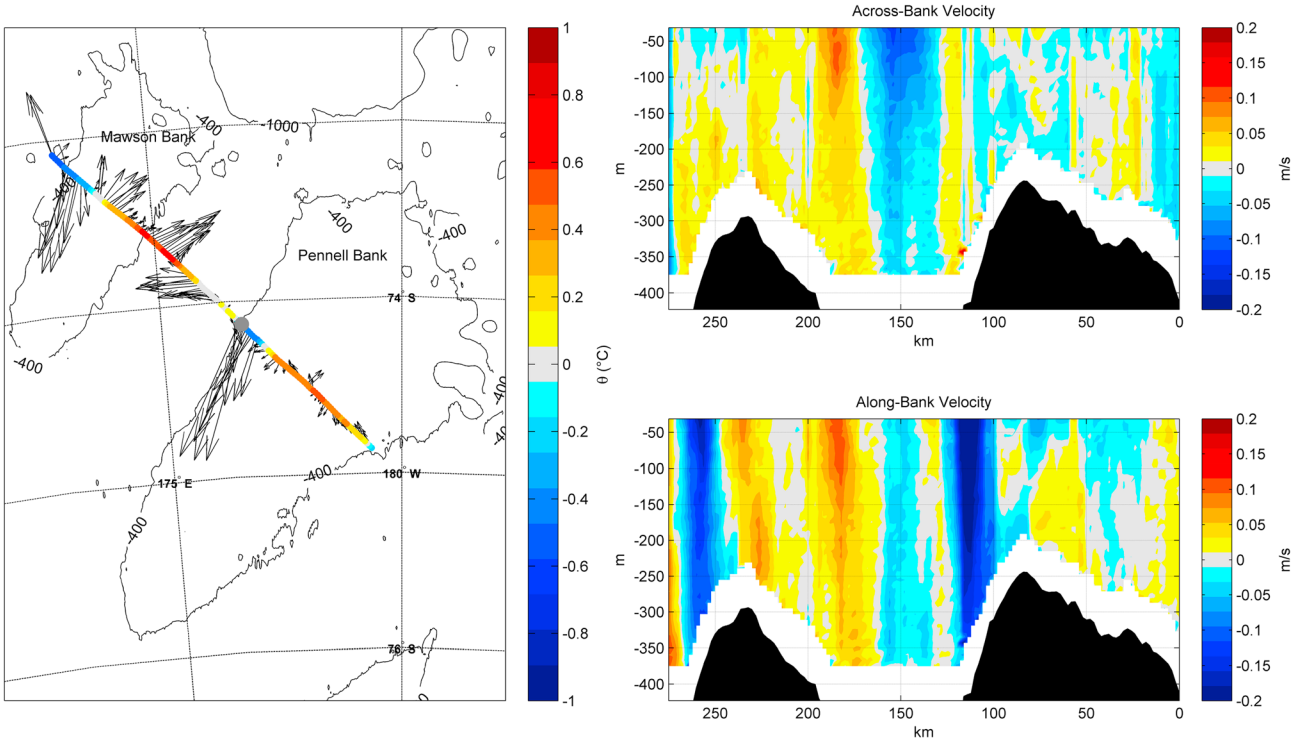

Figure 10. De-tided depth-averaged currents (black vectors) and surface temperature (colored track) over the across-bank section (left). The depth-dependent velocity sections (m/s) for the cross-bank (above right) and along-bank (below right) velocity components. These are the average of cross sections sampled between 22 January and 12 February 2011. The mooring location is shown as a gray circle (left).

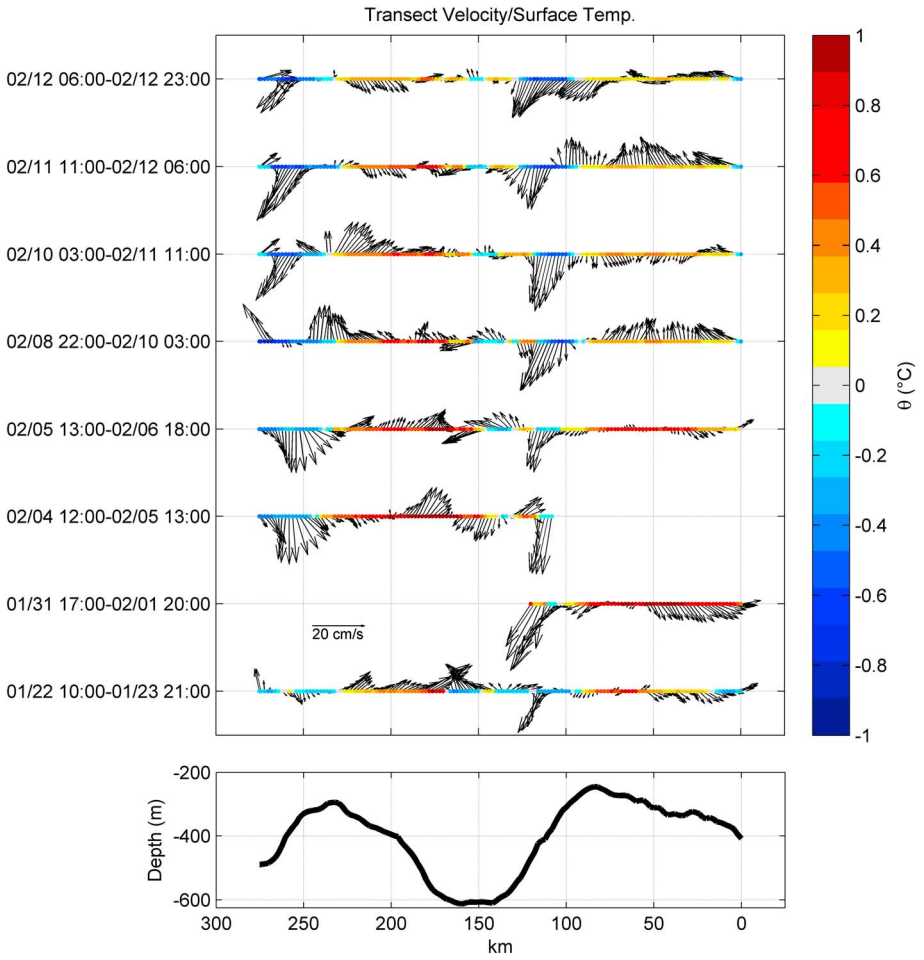

Figure 11. De-tided depth-averaged currents (black vectors) and surface temperature (colored track) for each of the across-bank sections. The topography identifying Pennell Bank (right) and Mawson Bank (left) is also shown (bottom).

present during the stronger spring tide. Throughout the record, there are also significant potential temperature shifts between −0.3°C and −1.6°C over periods much less than a day. The different response between the potential temperature and salinity time series at this depth is likely due to the difference in their vertical gradients and the relative influence each has on the density. At these salinity and temperature ranges, the ratio of beta to alpha is about 18 (beta ~ $d\rho/dS$, alpha ~ $d\rho/d\Theta$, where ρ is density, S is salinity, and Θ is potential temperature). Thus, fairly large excursions in potential temperature relative to salinity are to be expected. This is most evident at depth where there are large thermal gradients associated with MCDW. Here small vertical excursions lead to larger changes in potential temperature than salinity. The more gradual salinity changes with depth are seen only during the largest vertical excursions associated with the tides. The pressure data (not shown) indicate a fluctuation in the 225 m sensor depth of 10–30 m correlated with the tide. While significant, this sensor motion does not appear to account for all the variability in the diurnal band.

[24] The glider data collected in the vicinity of the mooring provides a spatial context for this temporal variability. A glider subsection of the transect that begins in the deeper water of Joides Trough moves up the slope of Pennell Bank toward the 280 m isobath (Figure 13). In the deeper water of the trough, the water column is seen to be relatively consistent with a layer of MCDW approximately 200 m deep. As the glider approaches the shallower water of the bank, this layer of MCDW deflects significantly in the vertical between 200 m and 350 m. The time scale of the depth variation of MCDW is consistent with the dominant diurnal tide that peaks over the shallows of the banks near the shelf break. The dashed black line approximates the location of the mooring. The apparent movement of the MCDW layer through the water column explains in part the variation in the potential temperature time series at 230 m from the mooring. This MCDW feature along the bank is highly variable over time scales of hours. This variation sampled by the glider is likely the result of tidal forcing on a spatially varying potential temperature field observed in the ship data.

4. Discussion

[25] Modified deep water intruding onto the shelf is a potential source of heat and micro-nutrients to the Ross Sea. Therefore, the magnitude and direction of MCDW transport are needed to quantify its impact on the heat and micronutrient budgets that influence Ross Sea processes. Throughout

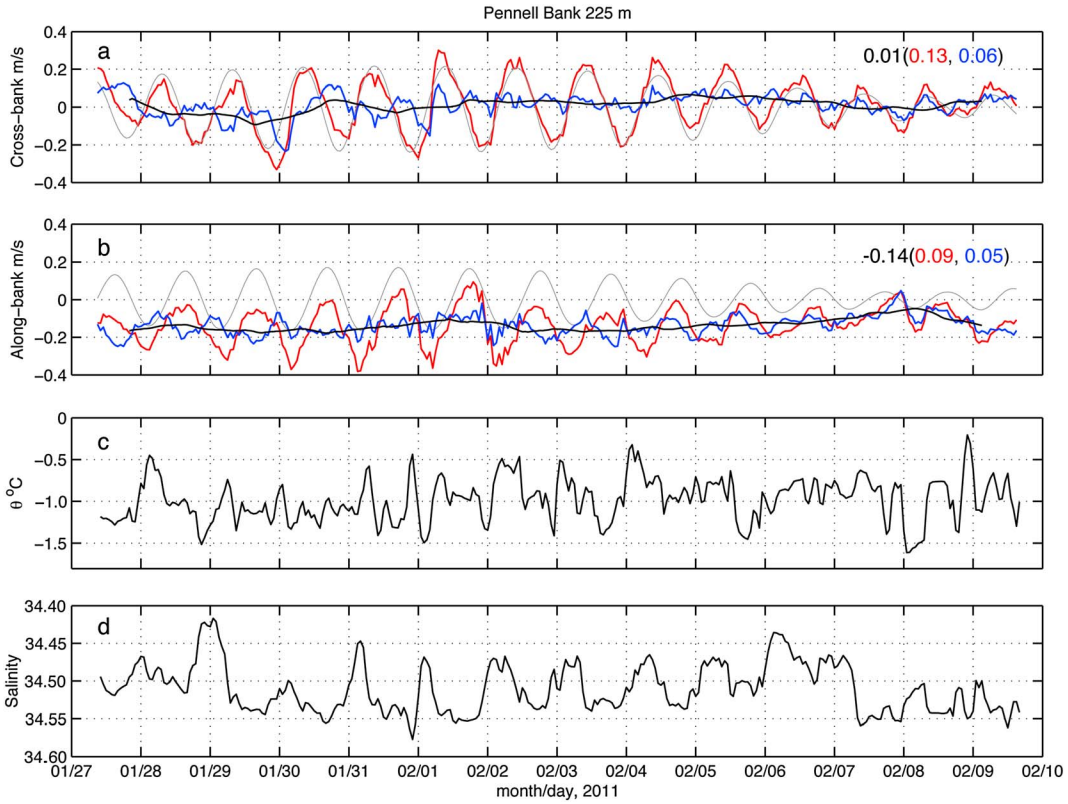

Figure 12. Moored hourly data including (a) cross-bank velocity (225 m), (b) along-bank velocity (225 m), (c) potential temperature (230 m), and (d) salinity (230 m). For Figures 12a and 12b, the red line is the hourly data, gray is velocity predicted by the barotropic tide model Ross_TIM [*Erofeeva, et al.*, 2005], blue is de-tided data, and black is the 25 h running mean of the hourly data. Record-length mean of the hourly velocities is given in the upper-right corner, with the standard deviation of the hourly (red) and de-tided (blue) velocities in parentheses.

our survey, a large phytoplankton bloom was sustained over Pennell Bank (Figure 14). Both satellite remote sensing and ship board sampling identified this surface feature centered over the north east corner of Pennell Bank. Given the observed variation in MCDW transport and the apparent separation between it and the bloom, we can use our targeted dataset to identify two possible pathways that link the MCDW source waters to the bloom. The first is a direct transport eastward near the shelf break between the MCDW core observed at the mooring and the adjacent bloom over Pennell Bank. The large vertical excursion of the MCDW seen in the glider section could elevate that source above the minimum depth of the bank enabling cross-isobath transport onto the bank. During the cruise, we sampled stations between the troughs and the shallows of the bank along a line that bisected the mooring location. Along this line, there is no evidence of MCDW moving up slope over shallower water. A station 30 km east of the MCDW core in 280 m of water (80 km on the x axis of Figure 9) shows a water column predominately composed of a warm surface layer over a cooler, saltier bottom layer (Figure 9). The peak temperature and oxygen minimum characteristic of MCDW is not seen in any of the profiles sampled at this station. Based on these station data and the weak vertical shear in the ADCP velocities along this line, it is unlikely that the MCDW intrusion seen over the 400 m isobath is directly mixing up to the shallows of the adjacent bank, even with the significant vertical excursions of up to 100 m related to the dominant diurnal tide.

[26] An alternative pathway for the MCDW is to continue south along the bank, moving gradually upslope along the way. Once near the southern edge of the bank, the MCDW could turn north, continuing to follow the 400 m isobath back toward the shelf break. There is evidence of this isobath following flow pattern in model simulations [*Dinniman et al.*, 2003]. This pathway is driven primarily by bathymetry given the mostly barotropic flow seen over the 400 m isobath. These model simulations are consistent with the mooring and ship-based ADCP data with a strong along isobath flow moving south over the 400 m isobath west of Pennell and Mawson Banks and a return flow back toward the shelf break on the eastern side of Mawson Bank. If we assume a barotropic flow following topography, we would expect the intrusion of MCDW over the 400 m isobath to be constrained by f/H, where f is the local Coriolis parameter and H is the water depth [*Marshall*, 1995]. Using the mooring site as an initial condition for the MCDW intrusion, we calculate the regions of the Ross Shelf that have consistent f/H values (Figure 15). If the MCDW is carried by a barotropic current south onto the shelf, then this flow would be limited to those areas shaded in tan. For Pennell Bank, we see the pathway continuing south and moving up onto the bank around the 74.5°S parallel where the steep slope of Pennell flattens. The shallower slope relaxes the dynamic constraint, allowing the MCDW to move up onto the bank. Once

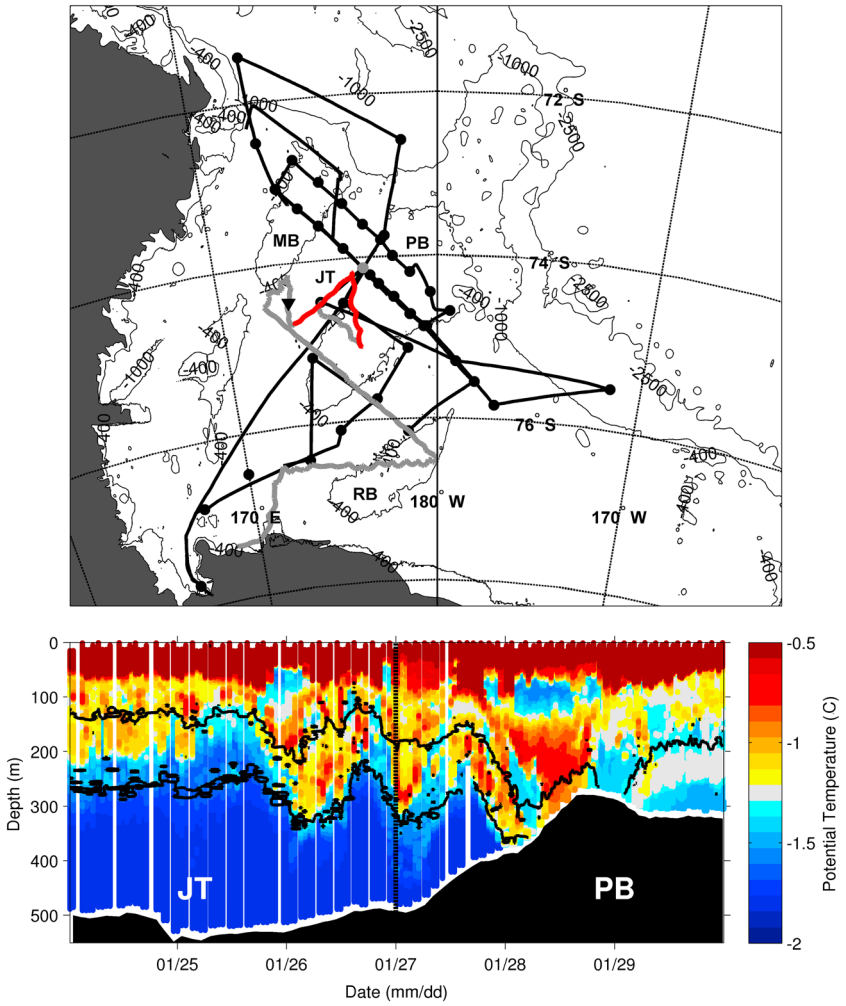

Figure 13. Subsection of the glider path that begins in Joides Trough and moves up the slope of Pennell Bank (red, above). Potential temperature along this section (below). The neutral density bounds defining MCDW are shown in black, and the topographic features are labeled as in Figure 1. The vertical dashed line (below) coincides with the sharp turn in the red transect (above).

over the bank, the MCDW is subject to the stronger diurnal tides and could be vertically mixed to the euphotic zone.

[27] The ADCP data identified a strong southward flow along the western edge of Pennell Bank coincident with the MCDW core. The depth-dependent data show that this flow is not truly barotropic. Given the observed shear, the *f*/H constraint may not apply to the MCDW intrusion along the bank. Recognizing that flow fields in the ocean are rarely fully barotropic, there is a modified denominator that considers the depth scale of the observed shear, f/F_o [*Krupitsky et al.*, 1996; *Gille*, 2003; *Gille et al.*, 2004], where

$$F_o = H_o(1 - \exp(-H/H_o)) \quad (1)$$

[28] H_o is the e-folding scale of the observed velocity shear:

$$v(z) = v(0)\ \exp(-z/H_o) \quad (2)$$

where $v(z)$ is the depth-dependent velocity, z is the depth of the measurement, and $v(0)$ is the magnitude of the surface velocity. Here we calculated H_o based on the average of the three velocity profiles within the MCDW core over the 400 m isobath (Figure 10). The exponential fit to this observed shear gives an e-folding depth scale of 380 m, approximately the depth of the water column. Since the shear is small, the modified constraint is not significantly different than the *f*/H constraint that assumes zero shear (not shown). With either definition, the flow transporting this MCDW from the shelf break onto the shelf likely follows the topography of both Pennell Bank and Mawson Bank toward the south. Unlike Pennell Bank, the water following Mawson is much less constrained to the slope and could quickly move over the shallows of the bank (Figure 15).

[29] Over Pennell Bank, there is a distinct separation between the MCDW core observed over the mooring site and the elevated chlorophyll concentrations over the shallower waters of the bank. The dynamic constraints shown in Figure 15 illustrate the isolation directly between them along ship sections sampled near the shelf break. Further south, however, the dynamic constraint relaxes and the glider section shows MCDW sliding up and over

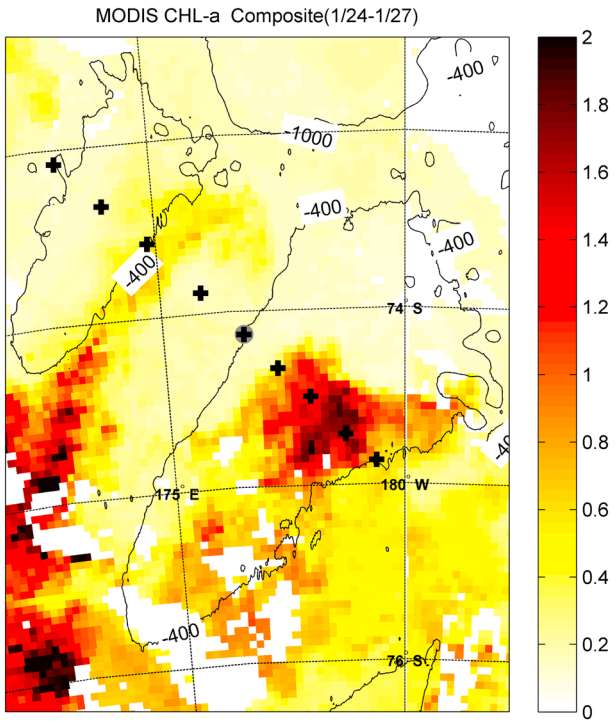

Figure 14. Surface map composite of satellite derived Chl-a concentration (mg/m^3). The cross-bank stations are shown as black crosses. The mooring location is also shown as a gray circle.

the bank (Figure 3). Once the MCDW reaches the shallows of the bank, it is subject to increased tides and could mix vertically toward the euphotic zone and the observed bloom. Through this pathway, the micronutrient supply of MCDW can reach the bloom and, if high enough concentration, help sustain its productivity.

5. Conclusion

[30] A multi-platform sampling strategy focused on the bank/trough topography near the outer shelf of the Ross Sea characterized the small scales that determine the transport of MCDW from preferred CDW intrusion sites at the shelf break south along the western slopes of both Pennell and Mawson Bank. For both banks, the MCDW signal is seen approximately over the 400 m isobath west of the banks. Using eight transects of ADCP sections across the bank/trough topography, we see a flow approximately barotropic moving southward along the bank. This flow is bringing with it cool fresher water on the surface and the warmer low oxygen water characteristic of MCDW at depth. The velocity and CTD sections averaged over eight cross sections were used to estimate a mean transport of MCDW over our survey of approximately 0.24 *Sv*. Both the glider and mooring data show that this mean transport is highly variable over scales of hours to days. The main variance, driven by the tides, appears to move this core of MCDW approximately 100 m in the water column every 12 h. At this point, we do not have the data coverage to determine the mechanism for this rapid movement of MCDW. However, we do conclude that this energetic tide is unlikely to drive the MCDW up and onto the Pennell Bank. Instead, given the small vertical shear in the flow, this intrusion of MCDW likely continues south along the bank until the slope flattens allowing the warmer mid-water to move over the bank. At that point, it is subject to the stronger tides of the bank and could be mixed up to the euphotic zone. The glider section across the southern edge of Pennell bank identifies the higher

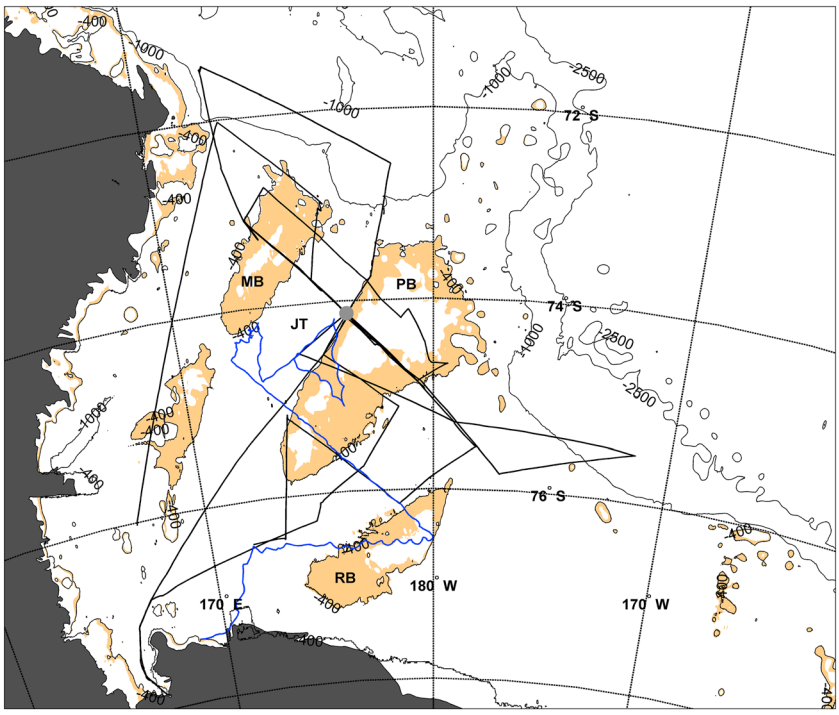

Figure 15. The regions of *f*/H (tan) consistent with the MCDW core identified in the vicinity of the mooring. The glider (blue) and ship track (black) are shown for reference. The mooring location is shown as a gray circle.

temperatures of the MCDW intrusion going up and over the bank. The scale of variability in time and space observed during this field study indicates a need for future study that incorporates longer time series, more detailed surveys, and eddy resolving models to fully describe the processes that govern the southward movement of MCDW into the Ross Sea.

[31] **Acknowledgments.** The NSF Office of Polar Programs (ANT-0839039) supported the Slocum Enhanced Adaptive Fe Algal Research in the Ross Sea (SEAFAReRS) project. The mooring was supported by the Cape Adare Long-term Moorings (CALM) project (ANT-0538148 and ANT-1141890). We want to specifically thank the project PIs for redeploying the mooring within days after recovery off Cape Adare. The successful deployment of the glider from the ice edge would not have been possible without the great effort of Chip Haldeman (Rutgers), Clayton Jones (Teledyne Webb Research), and Raytheon Polar Services. We would also like to thank the entire crew of the *RVIB Nathaniel B. Palmer* for their support throughout the cruise and John Kerfoot (Rutgers) for the glider processing before and after the deployment. This is Lamont-Doherty Earth Observatory contribution number 7662.

References

Arrigo, K. R., G. L. van Dijken, and S. Bushinsky (2008), Primary production in the Southern Ocean, 1997–2006, *J. Geophys. Res.*, *113*, C08004. doi:10.1029/2007JC004551.

Assmann, K., H. H. Hellmer, and A. Beckmann (2003), Seasonal variation in circulation and water mass distribution on the Ross Sea continental shelf, *Antarct. Sci.*, *15*(1), 3–11. doi:10.1017/S0954102003001007.

Assmann, K. M., and R. Timmermann (2005), Variability of dense water formation in the Ross Sea, *Ocean Dyn.*, *55*, 68–87.

Baines, P. G., and S. A. Condie (1998), Observations and modelling of Antarctic downslope flows: A review, *Antarct. Res. Ser.*, *75*, 29–49.

Budillon, G., and G. Spezie (2000), Thermohaline structure and variability in the Terra Nova Bay Polynya, Ross Sea, *Antarct. Sci.*, *12*, 493–508.

Budillon, G., P. Castagno, S. Aliani, G. Spezie, and L. Padman (2011), Thermohaline variability and Antarctic bottom water formation at the Ross Sea shelf break, *Deep Sea Res. I*, *58*, 1002–1018.

Dinniman, M. S., J. M. Klinck, and W. O. Smith (2003), Cross-shelf exchange in a model of the Ross Sea circulation and biogeochemistry, *Deep-Sea Res. II Top. Stud. Oceanogr.*, *50*(22–26), 3103–3120. doi:10.1016/j.dsr2.2003.07.011.

Erofeeva, S. Y., L. Padman, and G. Egbert (2005), Assimilation of ship-mounted ADCP data for barotropic tides: Application to the Ross Sea, *J. Atmos. Oceanic Technol.*, *22*(6), 721–734.

Foster, T. D., and E. C. Carmack (1976), Frontal zone mixing and Antarctic bottom water formation in the southern Weddell Sea, *Deep-Sea Res.*, *23*, 301–317.

Fragoso, G. M., and W. O. Smith (2012), Influence of hydrography on phytoplankton distribution in the Amundsen and Ross Seas, Antarctica, *J. Mar. Syst.*, *89*(1), 19–29. doi:10.1016/j.jmarsys.2011.07.008.

Fusco, G., G. Budillon, and G. Spezie (2009), Surface heat fluxes and thermohaline variability in the Ross Sea and in Terra Nova Bay polynyas, *Cont. Shelf Res.*, *29*, 1887–1895, doi:10.1016/j.csr.2009.07.006.

Gille, S. T. (2003), Float observations of the Southern Ocean: Part 1, Estimating mean fields, bottom velocities, and topographic steering, *J. Phys. Oceanogr.*, *33*, 1167–1181.

Gille, S. T., E. J. Metzger, and R. Tokmakian (2004), Sea floor topography and ocean circulation, *Oceanography*, *17*(1), 47–54.

Gordon, A. L., L. Padman, and A. Bergamasco (2009a), Southern Ocean shelf slope exchange, *Deep-Sea Res. II Top. Stud. Oceanogr.*, *56*(13–14), 775–777.

Gordon, A. L., A. H. Orsi, R. Muench, B. A. Huber, E. Zambianchi, and M. Visbeck (2009b), Western Ross Sea continental slope gravity currents, *Deep-Sea Res. II Top. Stud. Oceanogr.*, *56*(13–14), 796–817.

Hiscock, M. R. (2004), The regulation of primary productivity in the Southern Ocean. PhD Dissertation, Duke University, 150 pp.

Jacobs, S. S., and C. F. Giulivi (1998), Interannual ocean and sea ice variability in the Ross Sea. in Ocean, Ice, and atmosphere: Interactions at the Antarctic Continental Margin, edited by S. S. Jacobs, and R. F. Weiss, pp. 135–150, AGU.

Jacobs, S. (2004), Bottom water production and its links with the thermohaline circulation, *Antarct. Sci.*, *16*, 427–437.

Killworth, P. D. (1977), Mixing on the Weddell Sea continental slope, *Deep-Sea Res.*, *24*, 427–448.

Klinck, J. M., and M. S. Dinniman (2010), Exchange across the shelf break at high southern latitudes, *Ocean Sci.*, *6*(2), 513–524. doi:10.5194/os-6-513-2010.

Krupitsky, A., V. Kamenkovich, N. Naik, and M. A. Cane (1996), A linear equivalent barotropic model of the Antarctic Circumpolar Current with realistic coastlines and bottom topography, *J. Phys. Oceanogr.*, *26*, 1803–1824.

Marshall, D. (1995), Influence of topography on the large-scale ocean circulation, *J. Phys. Oceanogr.*, *25*, 1622–1635.

Muench, R., L. Padman, A. Gordon and A. Orsi (2009), A dense water outflow from the Ross Sea, Antarctica: Mixing and the contribution of tides, *J. Mar. Syst.*, *77*(4): 369–387.

Orsi, A. H., G. C. Johnson, and J. L. Bullister (1999), Circulation, mixing, and production of Antarctic Bottom Water, *Prog. Oceanogr.*, *43*(1), 55–109.

Orsi, A. H., W. M. Smethie, and J. L. Bullister (2002), On the total input of Antarctic waters to the deep ocean: A preliminary estimate from chlorofluorocarbon measurements, *J. Geophys. Res. Oceans*, *107*(3122), pp. 31-1–31-14.

Orsi, A. H., and C. L. Wiederwohl (2009), A recount of Ross Sea waters, *Deep-Sea Res. II Top. Stud. Oceanogr.*, *56*(13–14), 778–795.

Padman, L., S. Howard, A. Orsi, R. Muench (2009), Tides of the Northwestern Ross Sea and their impact on dense outflows of high salinity shelf water, in Deep-Sea Research AnSlope/Clima Topical Volume, edited by A. Gordon, L. Padman, A. Bergamasco, Southern Ocean Shelf Slope Exchange.

Rickard, G. J., M. J. Roberts, M. J. M. Williams, A. Dunn, and M. H. Smith (2010), Mean circulation and hydrography in the Ross Sea sector, Southern Ocean: Representation in numerical models, *Antarct. Sci.*, *22*(05), 533–558. doi:10.1017/s0954102010000246.

Robertson, R. (2005), Baroclinic and barotropic tides in the Ross Sea, *Antarct. Sci.*, *17*(1), 107–120. doi:10.1017/s0954102005002506.

Robertson, R., A. Beckmann, and H. Hellmer (2003), M2 tidal dynamics in the Ross Sea, *Antarct. Sci.*, *15*(1), 41–46. doi:10.1017/s0954102003001044.

Schofield, O., et al. (2007), Slocum Gliders: Robust and ready, *J. Field Rob.*, *24*(6), 1–14, doi:10:1009/rob.20200.

Smith, W. O., A. R. Shields, J. A. Peloquin, G. Catalano, S. Tozzi, M. S. Dinniman, and V. A. Asper (2006), Interannual variations in nutrients, net community production, and biogeochemical cycles in the Ross Sea, *Deep-Sea Res. II Top. Stud. Oceanogr.*, *53*(8–10), 815–833. doi:10.1016/j.dsr2.2006.02.014.

Whitworth, T., A. H. Orsi, S.-J. Kim, W. D. J. Nowlin, and R. A. Locarnini (1998), Water masses and mixing near the Antarctic Slope Front, *Ocean, Ice and Antarct. Res. Ser.*, *75*, 1–29.

Whitworth, T. III, and A. H. Orsi (2006), Antarctic Bottom Water production and export by tides in the Ross Sea, *Geophys. Res. Lett.*, *33*, L12609, doi:10.1029/2006GL026357.